Journal of Thermal Analysis and Calorimetry (2020) 140:2111–2122
https://doi.org/10.1007/s10973-019-08938-7

Functionalization graphene oxide with energetic groups as a new family of metal-free and energetic burning rate catalysts and desensitizers for ammonium perchlorate

Jian Cheng[1] · Jingchun Yan[2] · Lei Wang[1] · Rongxian Zhang[3] · Zuliang Liu[4] · Rui Wang[1] · Zhenming Li[1]

Received: 16 May 2019 / Accepted: 18 October 2019 / Published online: 11 November 2019

Abstract

A new family of metal-free and energetic graphene oxide (GO)-based burning rate catalysts (FGO **1–6**) with excellent catalytic and desensitization performances for ammonium perchlorate (AP) were synthesized by nucleophilic substitution reaction of energetic functional groups with acylated GO. The chemical structures, thermal stabilities, catalytic properties and desensitization performances of the functionalized GO were determined. It was shown that the functional groups on the nanosheets of GO imparted its energetic performance and thermal stability, and the catalytic properties and desensitization performances were also enhanced. The reduced mass loss rate along with enhanced residues formation indicated significant improvement in thermal stabilities for FGO **1–6** compared with GO. Besides, not only did FGO **1–6** lower the decomposition temperature, but also enhanced the overall heat for the thermal decomposition of AP. The FGO **1–6** decreased the exothermic peak of the high-temperature decomposition process of AP by 88.1, 93.4, 98.3, 85.8, 90.7 and 79.8 °C, corresponding to the decomposition heat of AP increased significantly from 655 to 2707, 2915, 3529, 3002, 3642 and 2718 J g^{-1}, which exhibited better catalytic activity than that of GO. In addition, the mechanical sensitivities of AP/GO and AP/FGO **1–6** mixtures decreased obviously in comparison with pure AP were also obtained.

Electronic supplementary material The online version of this article (https://doi.org/10.1007/s10973-019-08938-7) contains supplementary material, which is available to authorized users.

✉ Jian Cheng
chengjian09@foxmail.com

✉ Jingchun Yan
jcyan@issas.ac.cn

✉ Rui Wang
hades44@126.com

✉ Zhenming Li
lizmzf@163.com

[1] Department of Safety Science and Engineering, Zhejiang University of Technology, Hangzhou 310014, China

[2] Key Laboratory of Soil Environment and Pollution Remediation, Institute of Soil Science, Chinese Academy of Sciences, Nanjing 210008, China

[3] School of Chemistry and Chemical Engineering, Jiangsu University, Zhenjiang 212013, China

[4] School of Chemical Engineering, Nanjing University of Science and Technology, Nanjing 210094, China

Graphic abstract

A new family of metal-free and energetic GO-based burning rate catalysts with excellent catalytic properties and desensitization performances for ammonium perchlorate were developed.

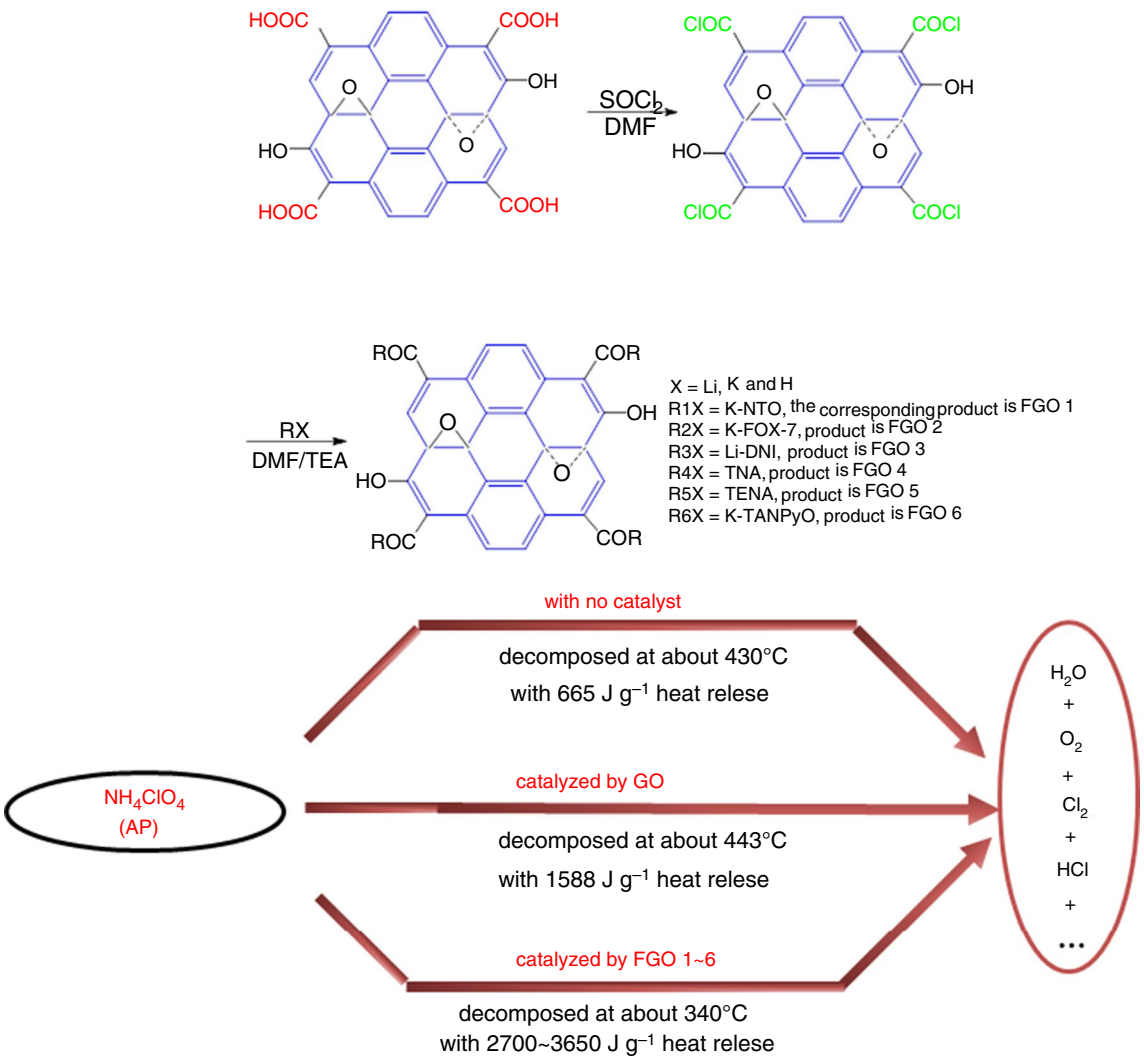

Keywords Graphene oxide · Functionalization · Ammonium perchlorate · Thermal decomposition · Mechanical sensitivity

List of symbols

GO	Graphene oxides
FGO	Functionalized graphene oxide
AP	Ammonium perchlorate
CMGO	Chemically modified graphene oxides
CSP	Composite solid propellants
HTPB	Hydroxyl-terminated polybutadiene
HMX	1,3,5,7-Tetranitro-1,3,5,7-tetraazacyclooctane
RDX	1,3,5-Trinitro-1,3 5-triazine
CL-20	Hexanitrohexaazaisowurtzitane
TNA	2,4,6-Trinitroaniline
TENA	2,3,4,6-Tetranitroaniline
NTO	3-Nitro-1,2,4-triazole-5-one
TANPyO	2,4,6-Triamino-3,5-dinitropyridine-1-oxide
FOX-7	1,1-Diamino-2,2-dinitroethylene
DNI	2,4-Dinitroimidazole
AGO	Acylated graphene oxides
DMF	*N*,*N*-dimethyl-formamide
LTD	Low-temperature decomposition
HTD	High-temperature decomposition
TNT	Trinitrotoluene
E_a	Activation energy

Introduction

CSP are widely used in a variety of aerospace and military applications, such as launch vehicles for spacecraft, satellites as well as in modern and advanced missile systems [1–5]. The CSP formulations mostly contain AP as an oxidizer and aluminum powder as metal fuel. The AP and aluminum powder particles are commonly held together by a binder called HTPB, which is also a less energetic fuel compared with metal. Additional ingredients for improving the properties of the propellants are burning rate catalysts, bonding agents, plasticizers and cure catalyst [1]. The combustion behavior of CSP is sensitive to the burning rate catalysts, which can influence the pressure exponent and burning rate [6–8]. Due to the limitation of loading characteristics of the CSP, it is critical to improve the decomposition efficiency of AP to achieve high-energy generation at low burning temperature. Transition metals, metal oxides and complex oxides are commonly used as burning rate catalysts in the thermal decomposition of AP [9–11]. However, the catalysts were non-energetic and would decrease the total energy of the propellants, which was one of the most important performance parameters. To overcome the disadvantage of the non-energetic burning rate catalysts, various energetic burning rate catalysts such as energetic complexes and salts with high catalytic activities were developed [12–18]. Although the energetic burning rate catalysts could overcome the above deficiencies, the disadvantages of high toxicity of heavy metal ions and produced solid oxide were still existed in combustion, which resulted in environmental pollution, especially high signature in combustion process. The signature is important in modern and advanced missile systems as detection of military launch location is an area of primary concern [19]. The high signature of CSP in combustion process would greatly affect the stealth and penetration abilities of the modern and advanced missile systems. Furthermore, due to the development of low vulnerability munitions, the safety problem of the CSP during their manufacture, storage, transportation and operation processes has attracted more and more attention. The main components of the CSP include AP and aluminum powder, leading to high sensitivity of the CSP. Meanwhile, in order to improve the energetic performance of CSP, increasing the high-energy contents (such as HMX, RDX and CL-20) in the CSP has brought about security issues [20]. The desensitization of AP has become one of the key technical ways to enhance the survivability of modern and advanced missile systems. Herein, it is highly desirable to develop environment-friendly, metal-free and energetic burning rate catalysts with good desensitization performance, which would become a new research field for the investigation of AP.

GO has plenty of oxygenic groups on the basal plane and the edge of the nanosheets, which offered tremendous opportunities to derive CMGO [21]. CMGO have significant interest in the scientific community due to their excellent mechanical, electrical and thermal properties, which were better than carbon nanotube and fullerene counterparts. It is worth pointing out that the advantages of metal-free GO and CMGO as "green" catalysts over the traditional metal-containing catalytic materials are environmentally friendly, inexpensive, biocompatible, stable and readily available [22–24]. Previous studies indicated that the presence of oxygenic groups enhanced the multifunctionality using GO as nanocatalyst support in solid propellants [25]. Besides, the mechanical sensitivity of high energetic materials was also reduced, due to the capability of GO to very efficiently dissipate mechanical shock, heat and electrostatic discharge on a molecular and a macromolecular level [26–28]. Noticeably, GO is deemed as a potential energetic additive for the solid propellants because it is thermally unstable and can readily undergo violent exothermic decomposition, producing amounts of heat [29]. GO has been utilized as nanocatalyst support to prepare nanocomposites with Co_3O_4, Mn_3O_4 and CuO, which exhibited extremely high catalytic activities on the thermal decomposition of AP [30–33]. Thus, it seems that GO could be used as an ideal multifunctionality additive in AP-based propellants. However, it was surprised that pristine GO exhibited almost weaker or no catalytic activities [30–33]. Although the GO-based nanocomposites had enhanced catalytic activity, there were also accompanying the common disadvantages. It is well known that TNA, TENA, NTO, TANPyO, FOX-7 and DNI (Fig. 1) were thermal stable aromatic multinitro compounds with good energetic and safety performances [34], which could be used as ideal intermediates to produce other new high-performance energetic materials by way of chemical transformation. To the best of our knowledge, covalent functionalization of GO with these functional groups was insensitive, heat resistant and high-energy energetic materials, which would derive a new family of CMGO, and might also impart GO with enhanced energetic performance and thermal stability, as well as catalytic activity on the thermal decomposition of AP. To date, few research articles have appeared using metal-free GO-based materials in the catalysis reaction of AP. In this study, a new family of high-energy materials functionalized GO (FGO **1–6**, Fig. 2) were synthesized by nucleophilic substitution reaction of TNA, TENA, potassium salts of NTO (K-NTO), TANPyO (K-TANPyO), FOX-7 (K-FOX-7) and lithium salt of DNI (Li-DNI) with AGO (Fig. 2). This work demonstrated the functional groups on the nanosheets surface of GO-enhanced energetic performance and thermal stability, as well as excellent catalytic and desensitization performances. This work provides a new

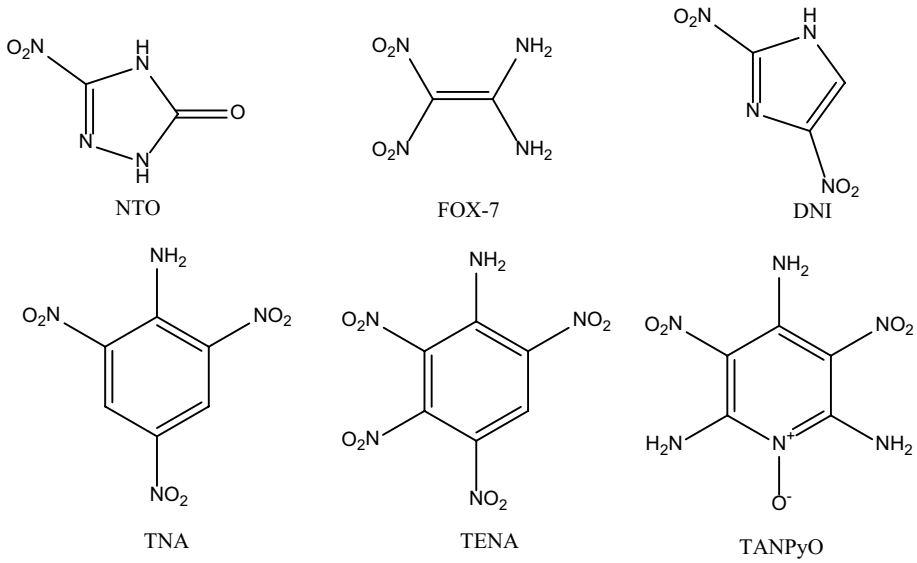

Fig. 1 Molecular structures of the functional groups

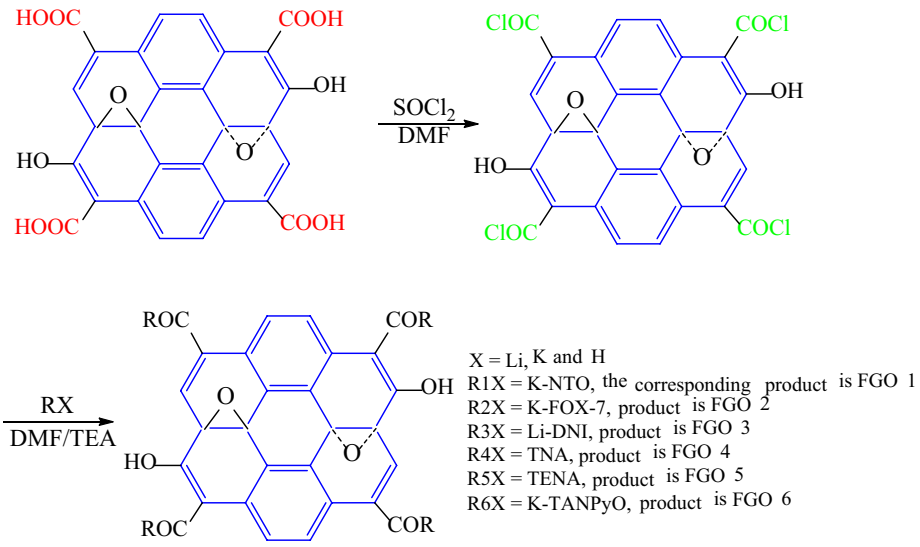

Fig. 2 Schematic picture of the preparation of FGO **1–6**

family of environment-friendly, metal-free, highly thermostable and energetic burning rate catalysts for the thermal decomposition of AP, which might point out the direction of research on the design and synthesis of burning rate catalysts in the future.

Materials and method

Materials and instrumentation

Thionyl chloride (99.9 mass%), DMF (99.8 mass%), triethylamine (99.9 mass%) and AP (AR, 99.5 mass%) were obtained from Aladdin (Shanghai, china). GO were purchased from commercial sources, purity ≥ 98 mass%, thickness, 1.0–1.77 nm, sheet diameter, 10–50 μm, layer, 1–5. All chemicals used were analytical grade, as received without further purification.

The FTIR analyses were conducted with use a Bruker (55FTIR) FTIR spectrometer (500–4000 cm^{-1}). Raman spectra were measured with a inVia spectrometer using a Ar laser ($\lambda = 514.5$ nm). XRD measurements were carried out on Bruker D8 Advance X-ray diffraction (Cu *K* radiation, $\lambda = 0.154178$ nm). XPS was performed with an American Thermo ESCALAB 250 electron spectrometer using Al Kα irradiation. DSC analyses were recorded on a TA-DSC-Q20 from 25 to 500 °C, and TG-DTG analyses were conducted on a TGA/SDTA851eMETTLER TOLEDO from 25 to 900 °C. The detailed microscopic structure and the chemical composition of the FGO **1–6** were investigated using high-resolution scanning transmission electron microscopes (Cs-corrected HR-STEM, JEM2010F and JEM2200FS operating at 200 kV, JEOL).

The conditions of TG-DTG and DSC were: sample mass, about 1.0–1.5 mg; N_2 flowing rate, 30 cm^3 min^{-1}; heating rates (β), 2.5, 5, 10 and 20 °C min^{-1}, furnace pressures, 0.1 MPa; reference sample, α-$A1_2O_3$; type of crucible, aluminum pan with a pierced lid.

Sensitivities toward impact and friction were tested using standard procedures [35, 36].

Synthesis of intermediates and FGO 1–6

General caution

TNA, TENA, K-NTO, K-TANPyO, K-FOX-7 and Li-DNI are energetic materials and tend to explode under certain conditions. Appropriate safety precautions should be taken during the synthesis, test and measurement processes, especially when these compounds are prepared on a large scale and in dry states.

Synthesis of intermediates

TNA [37], TENA [38], K-NTO [39], K-TANPyO [40], K-FOX-7 [41] and Li-DNI [42] were prepared according to the literature, and the procedures are shown in the Experimental Part in Supporting Information, respectively.

Synthesis of FGO 1–6

The mixture of 0.5 g GO, 200 mL thionyl chloride and 10 mL DMF was subject to a 500-mL three-necked flask and refluxed at 75 °C for 24 h in nitrogen atmosphere. The AGO was filtrated and washed three times by DMF and ice water, respectively, and dried at 75 °C under vacuum for 24 h. 0.3 g AGO was sonicated for 5 h in a 40 mL anhydrous DMF solution with 0.3–0.5 g intermediates. After 0.5 g triethylamine was added, the mixture was held at 100 °C under stirring for 48 h in a N_2 atmosphere. The synthesized FGO **1–6** products were filtrated and washed three times by DMF, and dried at 60 °C under vacuum for 48 h. Eventually, 0.25–0.35 g FGO **1–6** were obtained.

Preparation of AP/GO and AP/FGO 1–6 mixtures

AP mixtures (AP, d_{50}= 12.0 μm) were prepared by dry mixed for 48 h. The GO and FGO **1–6** contents in the AP mixture were 2.5 mass%.

Results and discussion

Structural characterization

In this work, FGO **1** was chosen as the representative compound to characterize the microstructures of these new carbon materials. Figure 3a–c shows the HRTEM images of FGO **1**, which indicated the layer structure of FGO **1** lamella. Meanwhile, the layered structure and wrinkled texture of graphene nanosheets were retained after modification. Elemental mapping analysis of FGO **1** in Fig. 3d–f also suggested the presence of C, N and O components in the FGO **1**. Figure 1S (Supporting Information) shows the FTIR spectra of GO and FGO **1–6**. For GO, the characteristic peaks appeared at 1722, 1621, 1405, 1223 and 1045 cm^{-1} were assigned to the carbonyl C=O, aromatic C=C, carboxy COOH, epoxy and C–O, respectively [43]. After modification, the peaks of the oxygenic groups were reduced significantly. A new weak peak at about 1650 cm^{-1} was corresponded to the amide carbonyl stretch, and a new weak peak at about 1560 cm^{-1} was for C–N in-plane stretching, which indicated that the functional groups were grafted onto the nanosheets of AGO by NH–CO and N–CO

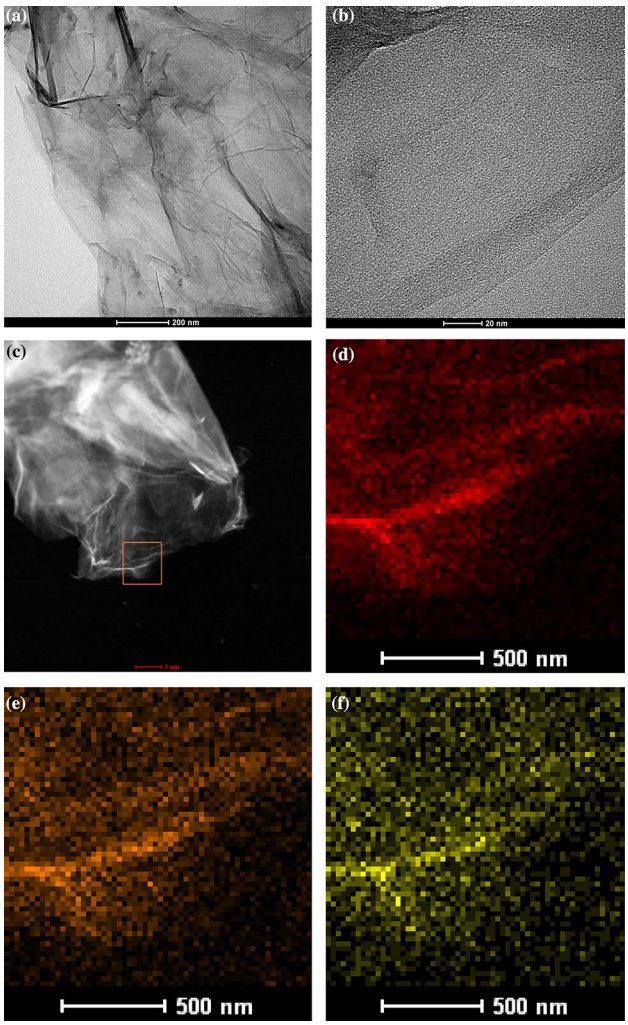

Fig. 3 HRTEM images of FGO **1** (**a**–**c**) and corresponding elemental mapping images of C, N, O (**d**–**f**)

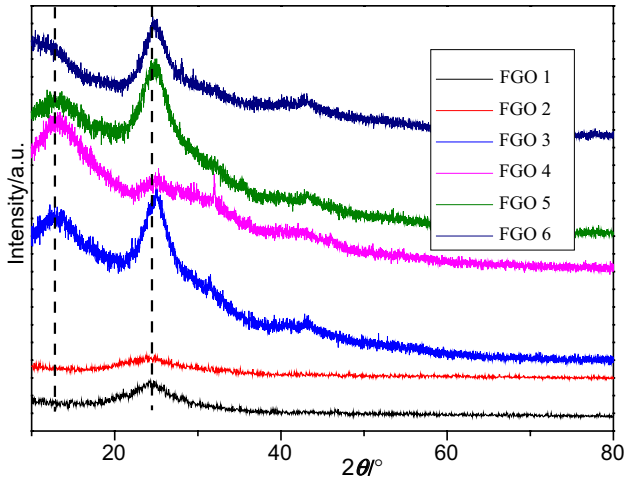

Fig. 4 XRD patterns of FGO **1–6**

bonds [44]. X-ray diffraction analysis was used to determine the crystalline structures of the FGO **1–6**. As shown in Fig. 4, all of the FGO **1–6** exhibited a peak centered at about 24.00°. Furthermore, FGO **3–6** exhibited a peak centered at about 10.00°, corresponding to the inter-planar spacing of GO [30], but for FGO **1** and **2**, the peak at the same position almost disappeared. The data obtained here revealed that some of the oxygenic groups on the FGO **1** and **2** had been removed during the acylation and modification process, but the basic structure of GO remained in the materials. Raman spectra of GO and FGO **1–6** were measured to give a more complete picture of the chemical bonding structure. As shown in Fig. 5, all GO and FGO **1–6** spectra exhibited two prominent bands at about 1356 and 1604 cm^{-1}, corresponding to the D-band and G-band of carbon materials, respectively. The D-band and G-band of FGO **1–6** were downshifted by 5, 6, 14, 9, 8, 7 and 21, 24, 34, 31, 29 cm^{-1} compared to that of GO sample, respectively. Furthermore, it was clear that the intensity ratios (I_D/I_G) of FGO **1–6** (1.05, 1.08, 1.10, 1.18, 0.99 and 1.17, respectively) were slightly increased compared with that of GO (0.82). The D-band raised from the structural imperfection, and the G-band corresponded to the band stretching of all pairs of sp^2 carbon atoms in both rings and chains [45]. The data obtained here were well agreed with the previous report [45], which suggested that the nanosheets of FGO **1–6** had higher defect content relative to the GO sample, while the basic structure of GO remained in these materials after functionalization. By XPS measurement, the chemical composition of FGO **1–6** can be further confirmed (XPS, Table 1 and Fig. 2S, Supporting Information). All of the FGO **1–6** showed new XPS peaks in N 1*s* and O 1*s* curves (at about 400.0 and 533.0 eV, respectively), which were attributed to the presence of NH–CO and N–CO bonds in these new carbon materials. This observation strongly supported our initial postulation that the functional groups were grafted to the nanosheets of AGO by nucleophilic substitution reactions. In addition, the N 1*s* and O 1*s* peaks at about 405.0 and 533.0 eV ($-NO_2$) were originated from the functional groups, since they were grafted to the nanosheets of AGO. The presence of the N 1*s* and O 1*s* peaks for the $-NO_2$ groups in FGO **1–6** indicated that nucleophilic substitution reactions between the functional groups and AGO indeed took place.

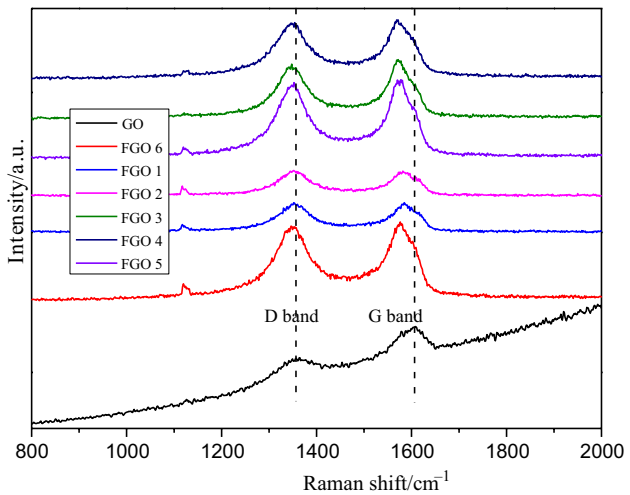

Fig. 5 Raman spectra of GO and FGO **1–6**

Thermal decomposition of GO and FGO 1–6

It is believed that GO is thermally unstable due to the oxygenic groups on the basal plane and the edge of the nanosheets [46, 47]. The lowered thermal stability can also be ascertained to the reduced van der Waals interaction between the layers [45]. As shown in Fig. 6 from the TG curve of GO, the mass loss for GO was initiated almost immediately above room temperature. The most severe mass loss for GO occurred at about 200 °C, which was due to the removal of oxygenic groups, and release of H_2O, CO and CO_2 [48]. By contrast, FGO **1–6** showed a difference thermal decomposition behaviors compared with that of GO. There was no significant mass loss for FGO **1–6** before 500 °C, and the most severe mass loss occurred at about 700 °C. The mass loss rate with temperature of FGO **1–6** was also significantly lower and extremely more residues were formed, indicating enhanced improvement in thermal stabilities of FGO **1–6**.

Table 1 The fitted N 1*s* and O 1*s* XPS spectra of the functional groups, GO and FGO **1–6**

Samples	N 1*s*/eV			O 1*s*/eV				
	NO_2	N(H)–CO	N=C	NO_2	N(H)–CO	C=O	C–OH	COOH
GO	–	–	–	–	–	531.8	531.1	532.4
NTO	405.6	–	400.4	532.0	–	530.7	–	–
FGO **1**	406.5	400.9	399.6	533.4	532.4	531.5	531.0	–
FOX-7	404.5	–	–	533.0	–	–	–	–
FGO **2**	404.0	400.0	–	534.7	533.2	531.8	530.8	–
Li-DNI	404.6	–	398.8	531.0	–	–	–	–
FGO **3**	405.7	399.8	398.9	534.1	533.2	531.9	530.9	–
TNA	405.1	–	–	533.1	–	–	–	–
FGO **4**	405.1	400.3	–	533.4	532.6	531.6	530.9	–
TENA	405.2	–	–	532.0	–	–	–	–
FGO **5**	405.8	399.9	–	533.4	532.9	531.8	531.0	–
K-TANPyO	405.8	–	398.8	530.7	–	–	–	–
FGO **6**	406.0	401.1	399.7	533.6	532.8	531.0	530.3	–

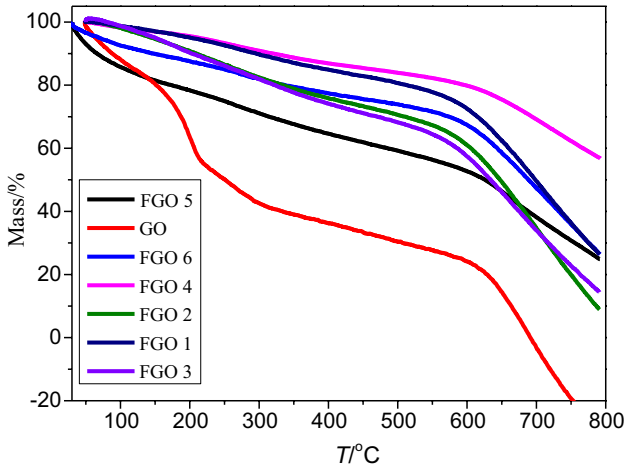

Fig. 6 TG curves of GO and FGO **1–6** at the heating rate of 10 °C min^{-1}

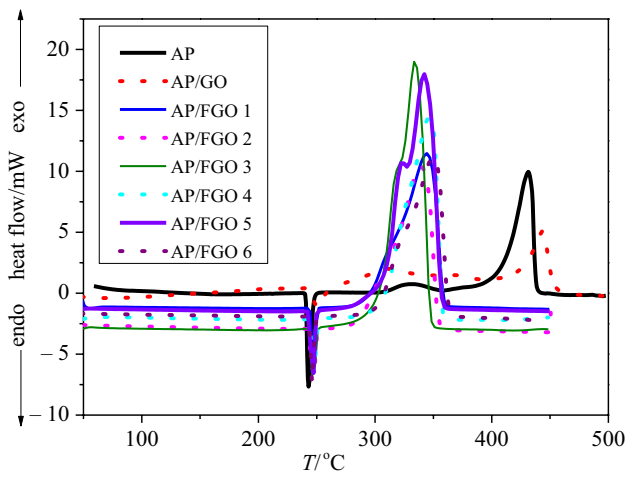

Fig. 7 DSC curves of pure AP, AP/GO and AP/FGO **1–6** at the heating rate of 10 °C min^{-1}

Catalytic effects of FGO 1–6 on the thermal decomposition of AP

To evaluate the potential application of FGO **1–6** used as burning rate catalysts in CSP, the catalytic effects of GO and FGO **1–6** on the thermal decomposition of AP were evaluated by using TG, DTG and DSC measurements and analyses (Figs. 7, 8 and Table 2). The thermal decomposition of pure AP (d_{50}= 12.0 μm) was studied in detail in our previous work [49]. As shown in Fig. 7, when GO was added, the thermal decomposition behavior of AP catalyzed by GO had no obvious changes compared with that of pure AP: The exothermic peak of LTD process for the AP/GO (312.3 °C) was 19.9 °C, which was slightly lower than that of pure AP. Strikingly, the exothermic peak of HTD process for the AP/GO (443.0 °C) was 10.5 °C, which was higher than that of pure AP. Furthermore, the TG and DTG curves of AP/GO exhibited that the thermal decomposition of AP/GO mixture started at higher temperature than that of pure AP in the temperature at about 375.0–450.0 °C. It seemed that GO exhibited somewhat negative catalytic effects. The overall heat for HTD and LTD processes (1588 J g^{-1}) was 933 J g^{-1}, which was higher than that of pure AP. The TG and DSC results of AP/GO indicated that GO exhibited almost no catalytic effects on the thermal decomposition of AP, which was well agreed with the previous work [30–33].

The DSC curves of AP/FGO **1–6** mixtures revealed that the addition of FGO **1–6** had no obvious effect on the crystal transition temperature, but lead to significant changes in the decomposition patterns. DSC curves of AP/

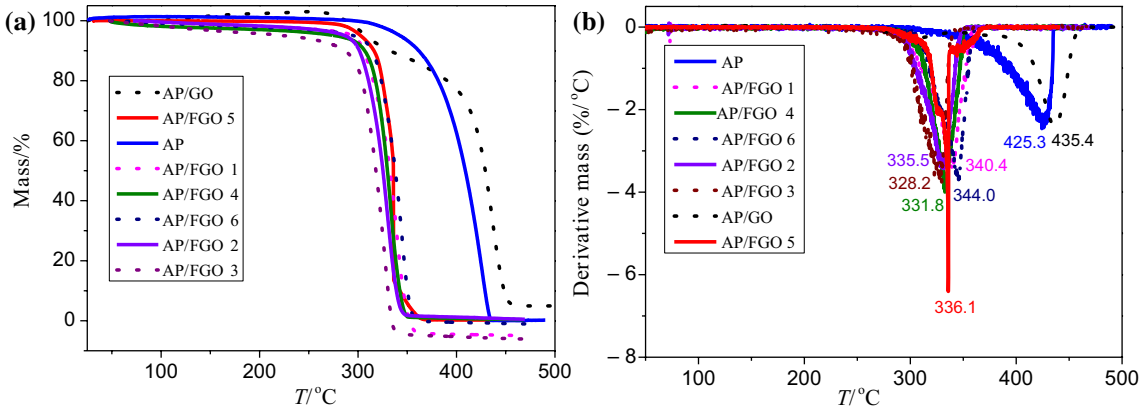

Fig. 8 TG (**a**) and DTG (**b**) curves of pure AP, AP/GO and AP/FGO **1–6** at the heating rate of 10 °C min^{-1}

Table 2 Summary of DSC results for pure AP, AP/GO and AP/FGO **1–6** in LTD and HTD processes at the heating rate of °C min^{-1}

Samples	ΔH/J g^{-1}	T_{endo}/°C	T_o/°C	T_p/°C	T_e/°C
Pure AP [49]	655	242.3	304.3, 363.1	332.2, 432.5	353.9, 443.6
AP/GO	1588	250.5	275.5, 406.4	312.3, 443.0	340.6, 462.9
AP/FGO **1**	2707	246.8	304.0	344.4	358.2
AP/FGO **2**	2915	246.7	302.2	339.1	353.4
AP/FGO **3**	3529	246.8	311.4	334.2	347.0
AP/FGO **4**	3002	247.2	306.9	346.7	357.6
AP/FGO **5**	3642	246.4	310.1	341.8	356.5
AP/FGO **6**	2718	246.4	303.7	352.7	362.5

T_{endo}, crystal transition temperature of DSC curve. T_o, onset temperature of decomposition for DSC curve. T_e, end temperature of decomposition for DSC curve. T_p, peak temperature of decomposition for DSC curve

FGO **1–6** mixtures showed a completely difference thermal decomposition behaviors compared to that of pure AP and AP/GO samples. Typically, the HTD process of AP/FGO **1–6** mixtures disappeared completely, and the thermal decomposition processes of AP/FGO **1–6** exhibited only a broad and flat peaks, with the peak temperature slightly higher than that of pure AP observed in LTD process. From Fig. 7, the LTD processes of AP containing FGO **1–6** mixtures (344.4, 339.1, 334.2, 346.7, 341.8 and 352.7 °C, respectively) were 88.1, 93.4, 98.3, 85.8, 90.7 and 79.8 °C, which were lower than that of pure AP. More notably, the decomposition heat of 2707, 2915, 3529, 3002, 3642 and 2718 J g^{-1} was observed in the presence of FGO **1–6**, about five times of the decomposition heat for pure AP, which could be a major breakthrough for the investigation of AP thermal decomposition. Meanwhile, the TG and DTG curves of AP/FGO **1–6** mixtures also indicated that the thermal decomposition of the mixtures proceeded in almost one step (only a peak at 340.4, 335.5, 328.2, 331.8, 336.1 and 344.0 °C in DTG curves, respectively), and the decomposition rate of AP was accelerated significantly in the presence of the FGO **1–6**. The date obtained was well agreed with the corresponding DSC results.

It is widely considered that addition of catalyst lowered the E_a of the reaction. A decrease in the E_a can be directly related to the catalytic activity of the catalyst from investigation. In the present work, FGO **6** was chosen as the representative compound to further evaluate the catalytic activity of these new carbon materials on the thermal decomposition of AP. The E_a value of the decomposition reaction of AP/FGO 6 mixture in LTD process was calculated following the Kissinger method [50], and the corresponding results are shown in Fig. 3S (Supporting Information) and Table 3. Compared with the results of our previous work [49], the E_a of thermal decomposition of AP decreased to 155.7 kJ mol^{-1} in LTD process in the

Table 3 Summary of DSC and kinetic parameters results of AP/FGO **6** in LTD process

Sample	β/°C min^{-1}	ΔH/J g^{-1}	T_p/°C	E_a/kJ mol^{-1}	R^2
AP/FGO **6**	2.5	1052	325.8	155.7 ± 4.7	0.9972
	5	1568	340.0		
	10	2718	352.7		
	20	3164	365.8		

presence of FGO 6. It could be seen that FGO 6 exhibited an obvious catalytic activity in the thermal decomposition of AP, which was consistent with the TG, DTG and DSC results. The above results revealed that the thermal decomposition of AP was accelerated significantly by addition of FGO **1–6**, and it is worth noting that the catalytic activities of FGO **3** and **5** were more active than the others.

The catalysis activities of various burning rate catalysts (transition metals, metal oxides, complex oxides, energetic complexes/salts and some nanocomposites) on the thermal decomposition of AP have been fully evaluated in the studies [9, 51]. However, all of the above burning rate catalysts have common disadvantages, that is, the existence of heavy metal ions, resulted in environmental pollution and high signature in combustion process. In contrast, not only did FGO **1–6** lower the decomposition temperature, but also significantly enhanced the overall heat for the thermal decomposition of AP. Besides, FGO **1–6** could effectively avoid the defect of metal-containing burning rate catalysts. In conclusion, FGO **1–6** could be used as metal-free and energetic burning rate catalysts in AP-based CSP.

Possible thermal decomposition path ways of AP catalyzed by FGO 1–6

It is interesting to note that when the typical carbon materials (graphene, GO and carbon nanotubes) were utilized as nanocatalyst support for transition metals, metal oxides and energetic complexes, which exhibited extremely high catalytic activities on the thermal decomposition of AP [30–33, 49]. However, all of these pristine carbon materials showed weaker or no catalytic activities [30–33]. GO was sensitive to heat because of the oxygen-containing groups on the basal plane and the edge of the sheets [46, 47]. The main decomposition of GO occurred in the temperature ranged about 200–300 °C, and left behind vacancies and topological defects throughout the nanosheets of reduced GO, which inevitably affected its electronic and mechanical properties and catalytic activity on the thermal decomposition of AP [47]. Compared with GO, the thermal stability of graphene and carbon nanotubes was significantly enhanced, while there was no obvious improvement in the catalytic activity of them. Amazingly, when the functional groups were covalently functionalized onto the nanosheets of GO, it imparted GO excellent catalytic activities. Furthermore, the DSC curves of AP/FGO **1–6** mixtures revealed that the transition stage between LTD and HTD processes of AP was completely disappeared, under the catalysis of FGO **1–6**. To the best of our knowledge, NH_3 played an important role in LTD process of pure AP, which increased the induction period and reduced the reaction rate and suppressed sublimation completely [7]. The incomplete oxidation of NH_3 was also the main reason for the formation of transition stage [7]. In addition, Liu et al. have found that HMX can accelerate the thermal decomposition of AP, and the main reason is that the product of NO_2 from HMX thermal decomposition can oxidize the NH_3 generated in AP dissociation process, speeding up the primary and secondary decomposition processes of AP [52]. It could be deduced that the functional groups on the nanosheets surface of GO might play a key role in the oxidative reaction between NH_3 and $HClO_4$. Based on the above results, a possible thermal decomposition path way of AP catalyzed by FGO **1–6** was proposed and is shown in Fig. 9.

In primary decomposition of AP/FGO **1–6** mixtures, FGO **1–6** were more likely to expose active sites to adsorb $HClO_4$ and NH_3 [53], which covered on the FGO **1–6** and AP surface. At the same time, the $–NO_2$ on the functional groups started to decompose and released some oxidizing gas (NO_2 or NO) [52, 54], as well as an amount of heat, which would oxidize the NH_3 [55, 56]. Thus, with the help of the oxidizing gas (NO_2 or NO), the incomplete oxidation and supersaturated atmosphere of NH_3 will not occur, which brings about the combination of LTD and HTD processes of AP, as well as disappearance of the transition stage. It would be an important step for the catalysis reaction of AP/FGO **1–6** mixtures. The excellent electrical conductivity and thermal stability of reduced GO possibly lead to improvement of heat and electron transfer during the thermal decomposition of AP/FGO **1–6** mixtures. The reduced GO also participated in the oxidation reaction with $HClO_4$, which served as a fuel and released an extra amount of heat [57]. The processes of NH_3 oxidation and transformation of O_2 to O_2^- would be accelerated. Therefore, the FGO **1–6** could speed up the primary and secondary decomposition processes of AP/FGO **1–6** mixtures and the synergistic effect of the functional groups and nanosheets of GO in FGO **1–6** molecules for the

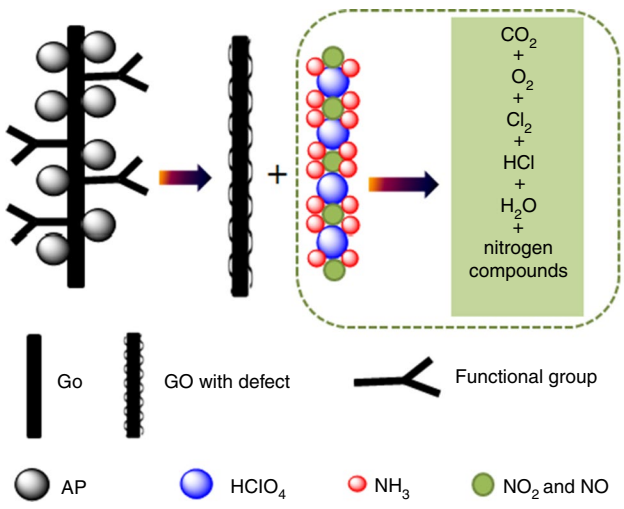

Fig. 9 Schematic of the thermal decomposition of AP catalyzed by FGO **1–6**

thermal decomposition of AP might be concluded. It should be note that how did the functional groups impart GO with catalytic activity on the thermal decomposition of AP were not clear yet, and further studies to explore the mechanism of thermal decomposition of AP catalyzed by FGO **1–6** are in progress.

Mechanical sensitivities of AP in the presence of GO and FGO 1–6

Previous researches have demonstrated that GO sheets have distinct advantage than fullerenes and carbon nanotubes as a desensitizer in explosives [59, 60], which were due to the efficiently dissipate mechanical shock, heat and electrostatic discharge on a molecular and a macromolecular level of GO. The mechanical sensitivity tests on the pure AP, AP/GO and AP/FGO **1–6** mixtures were performed to evaluate the desensitization performances of GO and FGO **1–6**, and the results are listed in Table 4. It was found that the impact and friction sensitivities of AP/GO and AP/FGO **1–6** mixtures decreased obviously in comparison with pure AP and RDX. When the mass ratio of GO and FGO **1–6** was 2.5 mass%, the impact and friction sensitivities of AP reduced from 8.0 to 12.8, 9.5, 11.7, 9.5, 9.4, 9.4, 12.3 J and 120 to 225, 206, 217, 198, 204, 205, 218 N, respectively. The obtained data revealed that the introduction of functional groups on the nanosheets of GO did not affect its basic structure and desensitization performances. The trend in desensitization performance for GO and FGO 1–6 was shown to be in the order of FGO **1** ≈ FGO **3** ≈ FGO **4** ≈ FGO **5** < FGO **2** ≈ FGO **6** < GO, probably due to desensitization effects of amino groups on the molecular structures of FGO **2** and FGO **6** [34].

Table 4 Mechanical sensitivities of AP, AP/GO and AP/FGO **1–6** mixtures, in comparison with TNT and RDX

Samples	Impact sensitivity/J	Friction sensitivity/N
Pure AP	8.0	120
AP/GO	12.8	225
AP/FGO **1**	9.5	206
AP/FGO **2**	11.7	217
AP/FGO **3**	9.5	198
AP/FGO **4**	9.4	204
AP/FGO **5**	9.4	205
AP/FGO **6**	12.3	218
TNT [58]	15.0	> 360
RDX [58]	7.5	120

Conclusions

In summary, a new family of metal-free, energetic and highly thermostable burning rate catalysts FGO **1–6** were synthesized and characterized. The data obtained revealed that the functional groups was grafted onto the nanosheets of GO by NH-CO and N-CO bonds. FGO **1–6** exhibited better catalytic activity on the thermal decomposition of AP in comparison with GO. Not only did FGO **1–6** lower the decomposition temperature, but also significantly enhanced the overall heat for the thermal decomposition of AP. The excellent catalytic activity of FGO **1–6** is likely attributed to the synergistic effect of the functional groups and the nanosheets of GO in FGO **1–6** molecules. The functional groups could accelerate the processes of NH_3 oxidation and transformation of O_2 to O_2^-, and the reduced GO possibly lead to the enhance of heat and electron transfer in the thermal decomposition of AP/FGO **1–6** mixtures, which would speed up the primary and secondary decomposition processes of AP mixtures. In addition, FGO 1–6 exhibited similar desensitization performance for the mechanical sensitivity of AP by comparing with GO. It can be anticipated that FGO **1–6** could be used as multifunctionality additives in the CSP. When FGO **1–6** were added into the CSP, the combustion behavior, energetic and safety performances would be greatly improved while the heavy metal-containing materials emissions during the combustion process will be significantly reduced as well.

Acknowledgements We gratefully acknowledge the financial support from Zhejiang University of Technology and Nanjing University of Science and Technology. This work is supported by National Natural Science Foundation of Zhejiang Province (Nos. LY14E030005 and LQ16E040002).

References

1. Boyars C, Klager K. Propellants manufacture, hazards, and testing. Washington: American Chemical Society; 1969. p. 88.
2. Trache D, Maggi F, Palmucci I, DeLuca LT. Thermal behavior and decomposition kinetics of composite solid propellants in the presence of amide burning rate suppressants. J Therm Anal Calorim. 2018;132:1601–15.
3. Trache D, Klapötke TM, Maiz L, Abd-Elghany M, DeLuca LT. Recent advances in new oxidizers for solid rocket propulsion. Green Chem. 2017;19:4711–36.
4. Trache D, Maggi F, Palmucci IT, DeLuca L, Khimeche K, Fassina M, Colombo G. Effect of amide-based compounds on the combustion characteristics of composite solid rocket propellants. Arab J Chem. 2015. https://doi.org/10.1016/j.arabjc.2015.11.016.

5. Mezroua A, Khimeche K, Lefebvre MH, Benziane M, Trache D. The influence of porosity of ammonium perchlorate (AP) on the thermomechanical and thermal properties of the AP/polyvinylchloride (PVC) composite propellants. J Therm Anal Calorim. 2014;116:279–86.
6. Juibari NM, Eslami A. Investigation of catalytic activity of $ZnAl_2O_4$ and ZnMn $_2O_4$ nanoparticles in the thermal decomposition of ammonium perchlorate. J Therm Anal Calorim. 2017;128:115–24.
7. Jacobs PWMC, Whitehead HM. Thermal decomposition of ammonium perchlorate. Chem Rev. 1969;69:551–90.
8. Sovizi MR, Fakhrpour G, Madram AR. Comparison of thermal degradation behavior of epoxy/ammonium perchlorate composite propellants. J Therm Anal Calorim. 2017;129:401–10.
9. Chaturvedi S, Dave PN. A review on the use of nanometals as catalysts for the thermal decomposition of ammonium perchlorate. J Saudi Chem Soc. 2013;17:135–49.
10. Pandas HM, Fazli M. Fabrication of MgO and ZnO nanoparticles by the aid of eggshell bioactive membrane and exploring their catalytic activities on thermal decomposition of ammonium perchlorate. J Therm Anal Calorim. 2018;131:2913–24.
11. Juibari NM, Eslami A. Green synthesis of $ZnCo_2O_4$ nanoparticles by Aloe albiflora extract and its application as catalyst on the thermal decomposition of ammonium perchlorate. J Therm Anal Calorim. 2017;130:1327–33.
12. Singh G, Felix SP. Studies of energetic compounds, part 29: effect of NTO and its salts on the combustion and condensed phase thermolysis of composite solid propellants, HTPB-AP. Combust Flame. 2003;132:422–32.
13. Cheng ZY, Zhang GF, Fan XZ, Bi FQ, Zhao FQ, Zhang WQ, Gao ZW. Synthesis, characterization, migration and catalytic effects of energetic ionic ferrocene compounds on thermal decomposition of main components of solid propellants. Inorg Chim Acta. 2014;421:191–9.
14. Xia ZQ, Chen SP, Wei Q, Qiao CF. Syntheses and characterization of energetic compounds constructed from alkaline earth metal cations (Sr and Ba) and 1,2-bis (tetrazol-5-yl) ethane. J Solid State Chem. 2011;184:1777–83.
15. Yang Q, Chen SP, Xie G, Gao SL. Synthesis and characterization of an energetic compound $Cu(Mtta)_2(NO_3)_2$ and effect on thermal decomposition of ammonium perchlorate. J Hazard Mater. 2011;197:199–203.
16. Liu JJ, Liu ZL, Cheng J. Synthesis, crystal structure and properties of a novel tetra-nuclear Cu complex of ANPyO. J Solid State Chem. 2013;197:198–203.
17. Liu JJ, Liu ZL, Cheng J, Fang D. Synthesis, crystal structure and properties of energetic complexes constructed from transition metal cations (Fe and Co) and ANPyO. RSC Adv. 2013;3:2917–23.
18. Liu JJ, Liu ZL, Cheng J, Fang D. Synthesis, crystal structure and catalytic effect on thermal decomposition of RDX and AP: an energetic coordination polymer $[Pb_2\ (C_5H_3N_5O_5)_2\ (NMP)\cdot NMP]_n$. J Solid State Chem. 2013;200:43–8.
19. Oommen C, Jain SR. Ammonium nitrate: a promising rocket propellant oxidizer. J Hazard Mater. 1999;67:253–81.
20. Bazaki H, Kubota N. Friction sensitivity mechanism of ammonium perchlorate composite propellants. Propellants Explos Pyrotech. 1991;16:43–7.
21. Chen D, Feng HB, Li JH. Graphene oxide: preparation, functionalization, and electrochemical applications. Chem Rev. 2012;112:6027–53.
22. Kong XK, Sun ZY, Chen M, Chen CL, Chen QW. Metal-free catalytic reduction of 4-nitrophenol to 4-aminophenol by N-doped graphene. Energ Environ Sci. 2013;6:3260–6.
23. Su CL, Acik M, Takai K, Lu J, Hao SJ, Zheng Y, Wu PP, Bao QL, Enoki T, Chabal YJ, Loh KP. Probing the catalytic activity of porous graphene oxide and the origin of this behavior. Nat Commun. 2012;3:1298.
24. Navalon S, Dhakshinamoorthy A, Alvaro M, Garcia H. Carbocatalysis by graphene-based materials. Chem Rev. 2014;114:6179–212.
25. Sabourin JL, Dabbs DM, Yetter RA, Dryer FL, Aksay IA. Functionalized graphene sheet colloids for enhanced fuel/propellant combustion. ACS Nano. 2009;3:3945–54.
26. Li R, Wang J, Shen JP, Hua C, Yang GC. Preparation and characterization of insensitive HMX/graphene oxide composites. Propellants Explos Pyrotech. 2013;38:798–804.
27. Yu L, Ren H, Guo XY, Jiang XB, Jiao QJ. A novel ε-HNIW-based insensitive high explosive incorporated with reduced graphene oxide. J Therm Anal Calorim. 2014;117:1187–99.
28. Wang JY, Ye BY, An CW, Wu BD, Li HQ, Wei YJ. Preparation and properties of surface-coated HMX with viton and graphene oxide. J Energy Mater. 2016;34:235–45.
29. Kuo KK, Risha GA, Evans BJ, Boyer E. Potential usage of energetic nano-sized powders for combustion and rocket propulsion. Mater Res Soc Symp Proc. 2004;800:3–14.
30. Li N, Geng ZF, Cao MH, Ren L, Zhao XY, Liu B, Tan Y, Hu CW. Well-dispersed ultrafine Mn_3O_4 nanoparticles on graphene as a promising catalyst for the thermal decomposition of ammonium perchlorate. Carbon. 2013;54:124–32.
31. Lan YF, Deng JK, Li GP, Luo YJ. Effect of preparation methods on the structure and catalytic thermal decomposition application of graphene/Fe_2O_3 nanocomposites. J Therm Anal Calorim. 2017;127:2173–9.
32. Zhu JW, Zeng GY, Nie FD, Xu XM, Chen S, Han QF, Wang X. Decorating graphene oxide with CuO nanoparticles in a water-isopropanol system. Nanoscale. 2010;2:988–94.
33. Xu C, Wang X, Zhu JW, Yang XJ, Lu LD. Deposition of Co_3O_4 nanoparticles onto exfoliated graphite oxide sheets. J Mater Chem. 2008;18:5625–9.
34. Pagoria PF, Lee GS, Mitchell AR, Schmidt RD. A review of energetic materials synthesis. Thermochim Acta. 2002;384:187–204.
35. Sabaté CM, Delalu H, Jeanneau E. Synthesis, characterization, and energetic properties of salts of the 1-cyanomethyl-1, 1-dimethylhydrazinium cation. Chem-Asian J. 2012;7:1085–95.
36. Sabaté CM, Delalu H, Jeanneau E. Energetic hydrazine-based salts with nitrogen-rich and oxidizing anions. Chem-Asian J. 2012;7:2080–9.
37. Spencer EY, Wright GF. Preparation of picramide. Can J Res. 1946;24:204–7.
38. Vanderah DJ. A parametric study of the synthesis of 2,3,4,6-tetranitroaniline. J Energy Mater. 1990;8:378–91.
39. Kulkarni PB, Reddy TS, Nair JK, Nazare AN, Talawar MB, Mukundan T, Asthana SN. Studies on salts of 3-nitro-1,2,4-triazol-5-one (NTO) and 2,4,6-trinitroanilino benzoic acid (TABA): potential energetic ballistic modifiers. J Hazard Mater. 2005;123:54–60.
40. Hollins RA, Merwin LH, Nissan RA, Wilson WS, Gilardi R. Aminonitropyridines and their N-oxides. J Heterocycl Chem. 1996;33:895–904.
41. Anniyappan M, Talawar MB, Gore GM, Venugopalan S, Gandhe BR. Synthesis, characterization and thermolysis of 1,1-diamino-2,2-dinitroethylene (FOX-7) and its salts. J Hazard Mater. 2006;137:812–9.
42. Zhang GF, Wang Y, Cai MY, Dai DM, Yan K, Ma AS, Chen P, Wang R, Li P, Yi JH, Zhao FQ, Li JZ, Fan XZ. Synthesis, structural characterization, and thermal properties of alkaline (earth) compounds derived from 2,4-dinitroimidazole. J Coord Chem. 2010;63:1480–91.
43. Chen WF, Yan LF, Bangal PR. Chemical reduction of graphene oxide to graphene by sulfur-containing compounds. J Phys Chem C. 2010;114:19885–90.

44. Ramanathan T, Fisher FT, Ruoff RS, Brinson LC. Amino-functionalized carbon nanotubes for binding to polymers and biological systems. Chem Mater. 2005;17:1290–5.
45. Kumar NA, Choi HJ, Shin YR, Chang DW, Dai L, Baek JB. Polyaniline-grafted reduced graphene oxide for efficient electrochemical supercapacitors. ACS Nano. 2012;6:1715–23.
46. Larciprete R, Fabris S, Sun T, Lacovig P, Baraldi A, Lizzit S. Dual path mechanism in the thermal reduction of graphene oxide. J Am Chem Soc. 2011;133:17315–21.
47. Dreyer DR, Park S, Bielawski CW, Ruoff RS. The chemistry of graphene oxide. Chem Soc Rev. 2010;39:228–40.
48. Qiu Y, Guo F, Hurt R, Külaots I. Explosive thermal reduction of graphene oxide-based materials: mechanism and safety implications. Carbon. 2014;72:215–23.
49. Cheng J, Zhang RX, Liu ZL, Li LX, Zhao FQ, Xu SY. Thermal decomposition mechanism of Co-ANPyO/CNTs nanocomposites and their application to the thermal decomposition of ammonium perchlorate. RSC Adv. 2015;5:50278–88.
50. Kissinger HE. Reaction kinetics in differential thermal analysis. Anal Chem. 1957;29:1702–6.
51. Cheng J, Zheng Y, Li ZM, Liu ZL, Li LX, Zhao FQ, Xu SY. Catalytic reaction of ammonium perchlorate with energetic cobalt complex of 2,6-diamino-3,5-dinitropyrazine-1-oxide during thermal decomposition process. J Therm Anal Calorim. 2017;129:1875–85.
52. Liu ZR, Yin CM, Kong YH, Zhao FQ, Luo Y, Zhou H. Interaction of ammonium perchlorate with HMX and RDX during decomposition. J Propuls Tech. 2000;21:70–3.
53. Mattson EC, Pande K, Unger M, Cui S, Lu G, Gajdardziska-Josifovska M, Hirschmugl CJ. Exploring adsorption and reactivity of NH_3 on reduced graphene oxide. J Phys Chem C. 2013;117:10698–707.
54. Brill TB, James KJ, Brill TB, James KJ. Kinetics and mechanisms of thermal decomposition of nitroaromatic explosives. Chem Rev. 1993;93:2667–92.
55. Bedford G, Thomas JH. Reaction between ammonia and nitrogen dioxide. J Chem Soc Farad Trans. 1972;68:2163–70.
56. Brill TB, Brush PJ, Patil DG. Thermal decomposition of energetic materials 58. Chemistry of ammonium nitrate and ammonium dinitramide near the burning surface temperature. Combust. Flame. 1993;92:178–86.
57. Han X, Sun YL, Wang TF, Lin ZK, Li SF, Zhao FQ, Ren XN, Han X, Sun YL, Wang TF, et al. Thermal decomposition of ammonium perchlorate based mixture with fullerenes. J Therm Anal Calorim. 2007;91:551–7.
58. Cohen A, Yang Y, Yan QL, Shlomovich A, Petrutik N, Burstein L, Gozin M. Highly thermostable and insensitive energetic hybrid coordination polymers based on graphene oxide-Cu(II) complex. Chem Mater. 2016;28:6118–26.
59. Chi Y, Huang H, Li JS. Influences of CNTs on Thermal decomposition and mechanical sensitivity of HMX. In: International autumn seminar on propellants, explosives and pyrotechnics (2005IASPEP), Beijing, China, October 25–28, 2005. p. 319–21.
60. Jin B, Peng RF, Chu SJ, Huang YM, Wang R. Thermal decomposition of ammonium perchlorate based mixture with fullerenes. Propellants Explos Pyrotech. 2008;33:454–8.